Research Article | Vol. 24, No. 26 | 26 Dec 2016 | OPTICS EXPRESS 29691

Optics EXPRESS

Optimal design and performance metric of broadband full-Stokes polarimeters with immunity to Poisson and Gaussian noise

TINGKUI MU,[1,2,*] ZEYU CHEN,[1] CHUNMIN ZHANG,[1] AND RONGGUANG LIANG[2]

[1]*Institute of Space Optics, School of Science, MOE Key Laboratory for Nonequilibrium Synthesis and Modulation of Condensed Matter, Xi'an Jiaotong University, Xi'an 710049, China*
[2]*College of Optical Sciences, University of Arizona, Tucson, Arizona 85721, USA*
[*]*tkmu@mail.xjtu.edu.cn*

Abstract: In this paper, the design, optimization and analysis of broadband full-Stokes polarimeters with immunity to both Poisson and Gaussian noise are presented. Different from the commonly-used optimization metrics such as, the condition number (CN), the equally weighted variance (EWV), or the polarimetric modulation efficiency (PME) for Gaussian noise, the optimally balanced condition for Poisson noise (BCPN) is, for the first time, proposed and used as a metric for the optimization of polarimeters. The numerical results show that the polarimeters optimized with the BCPN have immunity to both Poisson and Gaussian noise. The broadband polarimeters optimized from the BCPN are achromatic and have similar polarimetric modulation properties over the waveband, in contrast to the polychromatic polarimeters optimized from the CN, EWV and PME, whose polarimetric modulation properties vary with wavelength.

© 2016 Optical Society of America

OCIS codes: (260.5430) Polarization; (120.5410) Polarimetry; (110.5405) Polarimetric imaging.

References and links

1. B. Cairns, E. E. Russell, J. D. LaVeigne, and P. M. Tennant, "Research scanning polarimeter and airborne usage for remote sensing of aerosols," Proc. SPIE **5158**, 33–44 (2003).
2. S. Persh, Y. J. Shaham, O. Benami, B. Cairns, M. I. Mishchenko, J. D. Hein, and B. A. Fafaul, "Ground performance measurements of the Glory Aerosol Polarimetry Sensor," Proc. SPIE **7807**, 780703 (2010).
3. M. Boffety, H. Hu, and F. Goudail, "Contrast optimization in broadband passive polarimetric imaging," Opt. Lett. **39**(23), 6759–6762 (2014).
4. X. Meng, J. Li, D. Liu, and R. Zhu, "Fourier transform imaging spectropolarimeter using simultaneous polarization modulation," Opt. Lett. **38**(5), 778–780 (2013).
5. M. W. Kudenov, N. A. Hagen, E. L. Dereniak, and G. R. Gerhart, "Fourier transform channeled spectropolarimetry in the MWIR," Opt. Express **15**(20), 12792–12805 (2007).
6. J. Craven-Jones, M. W. Kudenov, M. G. Stapelbroek, and E. L. Dereniak, "Infrared hyperspectral imaging polarimeter using birefringent prisms," Appl. Opt. **50**(8), 1170–1185 (2011).
7. F. Snik, T. Karalidi, and C. U. Keller, "Spectral modulation for full linear polarimetry," Appl. Opt. **48**(7), 1337–1346 (2009).
8. G. van Harten, J. de Boer, J. H. H. Rietjens, A. Di Noia, F. Snik, H. Volten, J. M. Smit, O. P. Hasekamp, J. S. Henzing, and C. U. Keller, "Atmospheric aerosol characterization with a ground-based SPEX spectropolarimetric instrument," Atmos. Meas. Tech. **7**(12), 4341–4351 (2014).
9. T. Mu, C. Zhang, C. Jia, and W. Ren, "Static hyperspectral imaging polarimeter for full linear Stokes parameters," Opt. Express **20**(16), 18194–18201 (2012).
10. T. Mu, C. Zhang, W. Ren, and C. Jia, "Static polarization-difference interference imaging spectrometer," Opt. Lett. **37**(17), 3507–3509 (2012).
11. T. Mu, C. Zhang, C. Jia, W. Ren, L. Zhang, and Q. Li, "Alignment and retardance errors, and compensation of a stateed spectropolarimeter," Opt. Commun. **294**, 88–95 (2013).
12. M. Rodenhuis, F. Snik, G. Harten, J. Hoeijmakers, and C. U. Keller, "Five-dimensional optical instrumentation: combining polarimetry with time-resolved integral-field spectroscopy," Proc. SPIE **9099**, 90990L (2014).
13. F. Snik, J. Craven-Jones, M. Escuti, S. Fineschi, D. Harrington, A. Martino, D. Mawet, J. Riedi, and J. S. Tyo, "An Overview of Polarimetric Sensing Techniques and Technology with Applications to Different Research Fields," Proc. SPIE **9099**, 90990B (2014).

#277667 http://dx.doi.org/10.1364/OE.24.029691
Journal © 2016 Received 26 Sep 2016; revised 28 Nov 2016; accepted 9 Dec 2016; published 14 Dec 2016

Optics EXPRESS

14. J. S. Tyo, D. L. Goldstein, D. B. Chenault, and J. A. Shaw, "Review of passive imaging polarimetry for remote sensing applications," Appl. Opt. **45**(22), 5453–5469 (2006).
15. R. M. A. Azzam, "Stokes-vector and Mueller-matrix polarimetry [Invited]," J. Opt. Soc. Am. A **33**(7), 1396–1408 (2016).
16. S. Pancharatnam, "Achromatic combinations of birefringent plates. Part 2: An achromatic quarter-wave plate," Proc. Indian Acad. Sci. A **41**, 137–144 (1955).
17. J.-F. Donati, C. Catala, G. A. Wade, G. Gallou, G. Delaigue, and P. Rabou, "A dedicated polarimeter for the MuSiCoS échelle spectrograph," Astron. Astrophys. Suppl. Ser. **134**(1), 149–159 (1999).
18. Y. Ikeda, H. Akitaya, K. Matsuda, K. S. Kawabata, M. Seki, R. Hirata, and A. Okazaki, "Development of high resolution spectropolarimeter, LIPS," Proc. SPIE **4843**, 437–447 (2003).
19. D. M. Harrington, J. R. Kuhn, C. Sennhauser, E. J. Messersmith, and R. J. Thornton, "Achromatizing a Liquid-Crystal Spectropolarimeter: Retardance vs. Stokes-Based Calibration of HiVIS," PASP **122**(890), 420–438 (2010).
20. D. Gisler, A. Feller, and A. M. Gandorfer, "Achromatic liquid crystal polarimeter," Proc. SPIE **4843**, 45–54 (2003).
21. J. S. Tyo, "Noise equalization in Stokes parameter images obtained by use of variable-retardance polarimeters," Opt. Lett. **25**(16), 1198–1200 (2000).
22. P. A. Letnes, I. S. Nerbø, L. M. S. Aas, P. G. Ellingsen, and M. Kildemo, "Fast and optimal broad-band Stokes/Mueller polarimeter design by the use of a genetic algorithm," Opt. Express **18**(22), 23095–23103 (2010).
23. L. M. S. Aas, D. G. Skåre, P. G. Ellingsen, P. A. Letnes, and M. Kildemo, "Design, optimization and realization of a ferroelectric liquid crystal based Mueller matrix ellipsometer using a genetic algorithm," Thin Solid Films **571**, 522–526 (2014).
24. H. Gu, X. Chen, H. Jiang, C. Zhang, and S. Liu, "Optimal broadband Mueller matrix ellipsometer using multi-waveplates with flexibly oriented axes," J. Opt. **18**(2), 025702 (2016).
25. D. S. Sabatke, M. R. Descour, E. L. Dereniak, W. C. Sweatt, S. A. Kemme, and G. S. Phipps, "Optimization of retardance for a complete Stokes polarimeter," Opt. Lett. **25**(11), 802–804 (2000).
26. T. Mu, C. Zhang, Q. Li, and R. Liang, "Achromatization of waveplate for broadband polarimetric system," Opt. Lett. **40**(11), 2485–2488 (2015).
27. J. C. del Toro Iniesta and M. Collados, "Optimum modulation and demodulation matrices for solar polarimetry," Appl. Opt. **39**(10), 1637–1642 (2000).
28. C. Xu, Z. Qu, X. Zhang, C. Jin, and X. Yan, "Polarimeter with two ferroelectric liquid-crystal modulators attached to the Yunnan solar tower," Appl. Opt. **45**(33), 8428–8433 (2006).
29. A. G. de Wijn, S. Tomczyk, R. Casini, and P. G. Nelson, "The polychromatic polarimeter," Proc. SPIE **7735**, 77354A (2010).
30. S. Tomczyk, R. Casini, A. G. de Wijn, and P. G. Nelson, "Wavelength-diverse polarization modulators for Stokes polarimetry," Appl. Opt. **49**(18), 3580–3586 (2010).
31. F. Snik, G. van Harten, R. Navarro, P. Groot, L. Kaper, and A. de Wijn, "Design of a full-Stokes polarimeter for VLT/X-shooter," Proc. SPIE **8446**, 844625 (2012).
32. F. Snik, G. van Harten, A. S. Alenin, I. J. Vaughn, and J. S. Tyo, "A multi-domain full-Stokes polarimeter that is efficient for 300-2500nm spectropolarimetry," Proc. SPIE **9613**, 96130G (2015).
33. J. Vernet, H. Dekker, S. D'Odorico, E. Mason, P. Di Marcantonio, M. Downing, E. Elswijk, G. Finger, G. Fischer, F. Kerber, L. Kern, J. L. Lizon, C. Lucuix, V. Mainieri, A. Modigliani, F. Patat, S. Ramsay, P. Santin, M. Vidali, P. Groot, I. Guinouard, F. Hammer, L. Kaper, P. Kjærgaard-Rasmussen, R. Navarro, S. Randich, and F. Zerbi, "Performances of X-shooter, the new wide-band intermediate resolution spectrograph at the VLT," Proc. SPIE **7735**, 77351I (2010).
34. M. Pertenais, C. Neiner, L. P. Parès, P. Petit, F. Snik, and G. van Harten, "UVMag: Space UV and visible spectropolarimetry," Proc. SPIE **9144**, 91443B (2014).
35. C. Neiner, D. Baade, A. Fullerton, C. Gry, G. Hussain, A. Lèbre, J. Morin, P. Petit, J. O. Sundqvist, A. ud-Doula, A. A. Vidotto, and G. A. Wade, "UVMag: stellar formation, evolution, structure and environment with space UV and visible spectropolarimetry," Astrophys. Space Sci. **354**(1), 215–227 (2014).
36. D. F. Elmore, S. R. Sueoka, and R. Casini, "Performance of polarization modulation and calibration optics for the Daniel K. Inouye Solar Telescope," Proc. SPIE **9147**, 91470F (2014).
37. T. R. Rimmele, J. Wagner, S. Keil, D. Elmore, R. Hubbard, E. Hansen, M. Warner, P. Jeffers, L. Phelps, H. Marshall, B. Goodrich, K. Richards, S. Hegwer, R. Kneale, and J. Ditsler, "The Advanced Technology Solar Telescope: beginning construction of the world's largest solar telescope," Proc. SPIE **7733**, 77330G (2010).
38. A. Peinado, A. Lizana, J. Vidal, C. Iemmi, and J. Campos, "Optimization and performance criteria of a Stokes polarimeter based on two variable retarders," Opt. Express **18**(10), 9815–9830 (2010).
39. M. R. Foreman, A. Favaro, and A. Aiello, "Optimal frames for polarization state reconstruction," Phys. Rev. Lett. **115**(26), 263901 (2015).
40. H. Dong, M. Tang, and Y. Gong, "Noise properties of uniformly-rotating RRFP Stokes polarimeters," Opt. Express **21**(8), 9674–9690 (2013).
41. F. Goudail, "Noise minimization and equalization for Stokes polarimeters in the presence of signal-dependent Poisson shot noise," Opt. Lett. **34**(5), 647–649 (2009).

Optics EXPRESS

42. H. Hurwitz and C. Jones, "A new calculus for the treatment of optical systems II. proof of three general equivalence theorems," J. Opt. Soc. Am. A **31**(7), 493–499 (1941).
43. J. S. Tyo, "Design of optimal polarimeters: maximization of signal-to-noise ratio and minimization of systematic error," Appl. Opt. **41**(4), 619–630 (2002).
44. T. Mu, C. Zhang, Q. Li, and R. Liang, "Error analysis of single-snapshot full-Stokes division-of-aperture imaging polarimeters," Opt. Express **23**(8), 10822–10835 (2015).
45. T. Mu, Z. Chen, C. Zhang, and R. Liang, "Optimal configurations of full-Stokes polarimeter with immunity to both Poisson and Gaussian noise," J. Opt. **18**(5), 055702 (2016).
46. T. Mu, C. Zhang, Q. Li, Y. Wei, Q. Chen, and C. Jia, "Snapshot full-Stokes imaging spectropolarimetry based on division-of-aperture polarimetry and integral-field spectroscopy," Proc. SPIE **9298**, 92980D (2014).
47. T. Mu, C. Zhang, and R. Liang, "Demonstration of a snapshot full-Stokes division-of-aperture imaging polarimeter using Wollaston prism array," J. Opt. **17**(12), 125708 (2015).
48. P. Llull, G. Myhre, and S. Pau, "Lens array Stokes imaging polarimeter," Meas. Sci. Technol. **22**(6), 065901 (2011).
49. W. L. Hsu, G. Myhre, K. Balakrishnan, N. Brock, M. Ibn-Elhaj, and S. Pau, "Full-Stokes imaging polarimeter using an array of elliptical polarizer," Opt. Express **22**(3), 3063–3074 (2014).
50. T. York, R. Marinov, and V. Gruev, "260 frames-per-second 648x488 resolution division-of-focal-plane polarimeter with structural dynamics and tracking applications," Opt. Express **24**(8), 8243–8252 (2016).
51. D. K. Aitken and J. H. Hough, "Spectral modulation, or ripple, in retardation plates for linear and circular polarization," PASP **113**(788), 1300–1305 (2001).
52. M. Semel, "Spectropolarimetry and polarization-dependent fringes," A&A **401**(1), 1–14 (2003).
53. G. Ghosh, "Dispersion-equation coefficients for the refractive index and birefringence of calcite and quartz crystals," Opt. Commun. **163**(1-3), 95–102 (1999).

1. Introduction

Broadband polarimeters have the capability of measuring the state of polarization over a wide wavelength range [1–3]. They can combine with spectrometers to form spectropolarimeters, modulating spectrally-resolved polarization state in a variety of spectral lines [4–13]. To demodulate the full-Stokes vector that consists of four Stokes components (S_0, S_1, S_2, S_3), the polarimeters should have no less than four modulation states [14, 15]. Generally, the broadband polarimeters can be categorized into two types: achromatic and polychromatic polarimeters [12, 13]. The achromatic polarimeters are built from achromatic or superachromatic retarders that are made of a set of crystal retarders or liquid crystal variable retarders (LCVR) [16–20]. Since the retardance and azimuth of retarder are similar over the whole wavelength range, the polarimetric modulation properties of the instrument matrix of the achromatic polarimeters will be similar at each wavelength. However, the achromatic retarders with the residual errors in retardance and azimuth usually are not suitable for high accurate polarimeters.

In contrast, the polychromatic polarimeters are configured directly from a stack of retarders regardless of their achromatic capability [21–24]. The retardances and azimuths of retarders are optimized by using the specified metrics such as condition number (CN) [20–23], equally weighted variance (EWV) [25, 26], or polarization modulation efficiency (PME) [27–37]. These metrics are originally derived for optimizing polarimeters at a single wavelength, and subsequently are employed for the optimization of wide waveband polarimeters. Since there are two degrees of freedom (retardance and azimuth) in each polarization modulation state, the polarimetric modulation properties of the optimal polychromatic polarimeters usually vary with wavelength. Remarkably, these three metrics are based on the assumption that each modulation state has the same measurement uncertainty (such as Gaussian noise is dominant in the measurements), or the S_0 component of the incident Stokes vector is much larger than other components (S_0, S_1, S_2).

The numerical results show that the optimal CN ($\mathrm{CN}_2 = \sqrt{3}$) of 2-norm is not affected by increasing the number n of modulation channels [38], the analytical results show that the minimum CN ($\mathrm{CN}_F = \sqrt{20}$) of Frobenius norm is also independent of the number n of modulation channels [39]. Although the CN performs well for diagnosing the condition of **A**, it doesn't have the advantage of multiple measurements for error minimization as

Optics EXPRESS

demonstrated apparently by the EWV. The optimal value of the EWV has been analytically determined from a rotating-retarder full-Stokes polarimeter as $\mathrm{EWV} = 40/n$ [40], and it decreases with the increase of modulation channels. For the polarimeter with the same number of modulation channels, the optimal retardances for the minimization of the EWV are usually different from that for the equalization of the noise variances on the last three Stokes parameters [40]. Both the CN and EWV lack the operation on the noise distribution for individual Stokes parameters. In contrast, PME can be used to handle the noise distribution on individual Stokes parameters [27]. For an optimally balanced full-Stokes polarimeter, the efficiency for S_0 is $\mathrm{PME}_0 = 1/2$, and for $\forall k \in [1,3]$, S_k is $\mathrm{PME}_k = 1/2\sqrt{3}$. They are also independent of the number n of modulation channels. However, the above three figures of merit, CN, EWV and PME, are effective only when the signal-independent detector noise is dominant.

Practically, there are some situations where the signal-dependent Poisson photon noise is dominant, such as the case in photon counting systems or quantum detectors with a sufficient level of light. Under these situations the measurement uncertainty will depend on the incident states of polarization. The corresponding metrics are then expected to minimize and balance the Poisson noise. Fortunately, the theory for the equalization and minimization of Poisson noise has been presented by Goudail [41].

In this paper, we will propose a metric based on Goudail's theory, namely optimally balanced condition for Poisson noise (BCPN), for the optimization of the polarimeter in the presence of Poisson noise. The BCPN could lead to an achromatic polarimeter contrary to the CN, EWV and PME that usually lead to a polychromatic polarimeter. To the best of our knowledge, there is no any polarimeter that is designed and optimized using Goudail's theory and the proposed metric.

2. The matrix theory of a broadband full-Stokes polarimeter

The time-resolved broadband polarimeter usually comprises of a rotatable retarder stack followed by a fixed horizontally polarizer as shown in Fig. 1. A spectrometer can be used to record the intensities corresponding to all of modulation states at each wavelength. Then spectrally-resolved polarization states are recovered with data reduction matrix techniques. If the retarders are made of passive materials such as Mica, quartz, MgF_2 and sapphire, the retarder stack could be packed as a monoblock and mechanically rotated to obtain different modulation state. In contrast, if the retarders are made from active materials such as photoelastic polarimeters, Pockels cells, nematic or ferroelectric liquid crystals, the retarder stack could be electrically switched to get a number of modulation states.

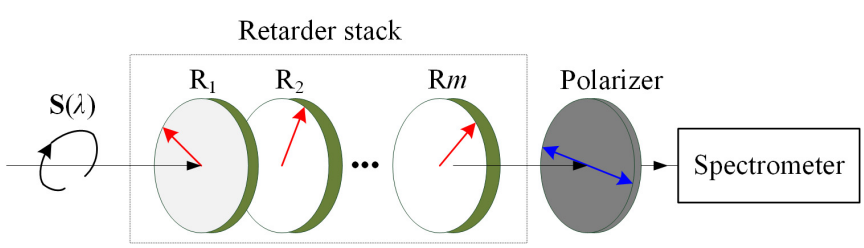

Fig. 1. The configuration of a broadband polarimeter which consists of m retarders.

Let us assume that the polarimeter consists of m retarders and the pth retarder's retardance and azimuth are (δ_p, θ_p). According to the Jones matrix theory [42], the retarder stack can be considered as a single retarder followed by a single rotator at each wavelength and the total Jones matrix is a unitary matrix,

Optics EXPRESS

$$\mathbf{U}(\lambda)=\mathbf{J}_{\mathrm{Ret}}(\delta_m,\theta_m)\cdots\mathbf{J}_{\mathrm{Ret}}(\delta_2,\theta_2)\mathbf{J}_{\mathrm{Ret}}(\delta_1,\theta_1)=\mathbf{J}_{\mathrm{Rot}}(\beta)\mathbf{J}_{\mathrm{Ret}}(\Phi,\alpha)=\begin{bmatrix}U_{11} & U_{12}\\ U_{21} & U_{22}\end{bmatrix} \tag{1}$$

where $\mathbf{J}_{\mathrm{Ret}}$ is the Jones matrix of a rotated retarder, and $\mathbf{J}_{\mathrm{Rot}}(\beta)$ denotes the Jones matrix of a rotator with an equivalent rotation angle β,

$$\mathbf{J}_{\mathrm{Rot}}=\begin{bmatrix}\cos\beta & -\sin\beta\\ \sin\beta & \cos\beta\end{bmatrix}. \tag{2}$$

Since the elements of the unitary matrix $\mathbf{U}$ obey $U_{22}=U_{11}^*$ and $U_{21}=-U_{12}^*$, the equivalent rotation angle β of the resulted rotator, the equivalent retardance Φ and azimuth α of the resulted retarder can be derived respectively as

$$\Phi=2\tan^{-1}\left(\sqrt{\frac{\mathrm{Im}^2(U_{11})+\mathrm{Im}^2(U_{21})}{\mathrm{Re}^2(U_{11})+\mathrm{Re}^2(U_{21})}}\right), \tag{3a}$$

$$\alpha=\frac{1}{2}\left[\tan^{-1}\left(\frac{\mathrm{Im}(U_{21})}{\mathrm{Im}(U_{11})}\right)-\tan^{-1}\left(\frac{\mathrm{Re}(U_{21})}{\mathrm{Re}(U_{11})}\right)\right], \tag{3b}$$

$$\beta=\tan^{-1}\left(\frac{\mathrm{Re}(U_{21})}{\mathrm{Re}(U_{11})}\right). \tag{3c}$$

If both the azimuth α and rotation angle β approach to zero and the retardance is close to a constant, the retarder stack will behave like an achromatic retarder.

Consequently, the ith modulation state of the polarimeter will be

$$\begin{aligned}\mathbf{a}_i(\lambda)&=[1\ \ 0\ \ 0\ \ 0]\mathbf{M}_{\mathrm{Pol}}(0)\mathbf{M}_{\mathrm{Ret}}(\delta_m,\theta_m)\cdots\mathbf{M}_{\mathrm{Ret}}(\delta_2,\theta_2)\mathbf{M}_{\mathrm{Ret}}(\delta_1,\theta_1),\\ &=[1\ \ 0\ \ 0\ \ 0]\mathbf{M}_{\mathrm{Pol}}(0)\mathbf{M}_{\mathrm{Rot}}(\beta)\mathbf{M}_{\mathrm{Ret}}(\Phi,\alpha)\end{aligned} \tag{4}$$

where $\mathbf{M}_{\mathrm{Ret}}$ and $\mathbf{M}_{\mathrm{Rot}}$ indicates the Muller matrices of a rotated retarder and a rotator respectively, and $\mathbf{M}_{\mathrm{Pol}}(0)$ denotes the Muller matrix of a horizontal polarizer. The vector $[1\ \ 0\ \ 0\ \ 0]$ is used to extract the first row of the total Muller matrix because it carries the measurement of intensity signal. Finally, the instrument matrix of the broadband polarimeter with n modulation states is

$$\mathbf{A}(\lambda)=\left[\mathbf{a}_1^T(\lambda)\quad \mathbf{a}_2^T(\lambda)\quad \cdots\quad \mathbf{a}_n^T(\lambda)\right]^T, \tag{5}$$

where T represents transpose operation, and $\mathbf{A}$ is the $n\times 4$ matrix with element A_{ik} (i = 1, 2,…, n ; k = 0, 1, 2, 3). If the retarder stack acts as a standard achromatic retarder, the instrument matrix $\mathbf{A}$ will be similar at each wavelength. That is the polarimeter has similar polarimetric modulation properties over the designed waveband. In contrast, if the instrument matrix $\mathbf{A}$ varies with wavelength but satisfies the optimization metrics CN, EWV or PME, the polarimeter is considered a polychromatic one.

For the input Stokes vector $\mathbf{S}$ with four components S_k, the measurement intensity vector $\mathbf{I}$ includes n measurement intensities is $\mathbf{I}=\mathbf{AS}$ [15], and the measurement intensity at each modulation state is

Optics EXPRESS

$$I_i = \sum_{k=0}^{3} A_{i,k} S_k . \tag{6}$$

The incident Stokes vector $\mathbf{S}$ is then estimated by $\hat{\mathbf{S}} = \mathbf{BI}$ and each estimated Stokes parameter is [15]

$$\hat{S}_k = \sum_{i=1}^{n} B_{k,i} I_i , \tag{7}$$

where $\mathbf{B}$ is the data reduction matrix. If $n = 4$, $\mathbf{B}$ is the classical inverse as $\mathbf{B} = \mathbf{A}^{-1}$ and $\hat{\mathbf{S}}$ is the optimal estimator. If $n > 4$, $\mathbf{B}$ is the pseudoinverse as $\mathbf{B} = \left(\mathbf{A}^T \mathbf{A}\right)^{-1} \mathbf{A}^T$ and $\hat{\mathbf{S}}$ is the least square estimator. Usually, the measurement intensity vector $\mathbf{I}$ is inevitably affected by the noise. Assuming the variance of noise in the ith measurement intensity is $\sigma_{I_i}^2$ and the noise in each measured intensity is statistically independent from the others, we can use the standard error propagation equation $\sigma_{S_k}^2 = \sum_{i=0}^{n} \left(\partial S_k / \partial I_i\right)^2 \sigma_{I_i}^2$ to derive the variance $\sigma_{S_k}^2$ on each estimated Stokes parameter as [43, 44]

$$\sigma_{S_k}^2 = \sum_{i=1}^{n} B_{k,i}^2 \sigma_{I_i}^2 . \tag{8}$$

Since the uncertainty of the estimator $\hat{\mathbf{S}}$ depends on the noise type in the measured intensity vector $\mathbf{I}$, the instrument matrix $\mathbf{A}$ with good condition and minimum error propagation for different noise is required over the whole wavelength region.

3. Optimization metrics for Gaussian and Poisson noise

If the measurement intensities are affected by the signal-dependent Poisson noise, the noise variance will be equal to the mean value,

$$\sigma_{I_i}^2 = \langle I_i \rangle = \sum_{j=0}^{3} A_{i,j} S_j . \tag{9}$$

The variance on each estimated Stokes parameter could be derived as [38]

$$\sigma_{S_k}^2 = \sum_{i=1}^{n} B_{k,i}^2 \sum_{j=0}^{3} A_{i,j} S_j = \sum_{j=0}^{3} Q_{k,j} S_j , \tag{10}$$

where $Q_{k,j} = \sum_{i=1}^{n} B_{k,i}^2 A_{i,j}$. If the incident Stokes vector is $\mathbf{S} = I_0 [1, P\mathbf{s}^T]^T$, the variance is rewritten as [41]

$$\sigma_{S_k}^2 = I_0 \left(Q_{k,0} + P\mathbf{q}_k \cdot \mathbf{s}\right). \tag{11}$$

with $\mathbf{q}_k = (Q_{k,1}, Q_{k,2}, Q_{k,3})$, the degree of polarization P , and the normalized Stokes vector $\mathbf{s}$. Obviously, both of them depend on the incident polarization state P . The maximum and minimum variances are then obtained respectively as [41]

$$(\sigma_{S_k}^2)_{\max} = I_0 \left(Q_{k,0} + P\|\mathbf{q}_k\|\right), \ (\sigma_{S_k}^2)_{\min} = I_0 \left(Q_{k,0} - P\|\mathbf{q}_k\|\right) \tag{12}$$

Goudail [41] has considered a particular case with $n = 4$ modulation states and pointed out the optimally balanced instrument matrix as

Optics EXPRESS

$$\mathbf{A}=\frac{1}{2}\begin{bmatrix}1 & 1/\sqrt{3} & -1/\sqrt{3} & -1/\sqrt{3}\\ 1 & 1/\sqrt{3} & 1/\sqrt{3} & 1/\sqrt{3}\\ 1 & -1/\sqrt{3} & 1/\sqrt{3} & -1/\sqrt{3}\\ 1 & -1/\sqrt{3} & -1/\sqrt{3} & 1/\sqrt{3}\end{bmatrix}. \tag{13}$$

With this ideal instrument matrix, the variances become independent of the input polarization state P and the total variance reaches its minima. Recently, we proposed a special merit function and several optimal configurations for a single wavelength based the ideal instrument matrix [45]. However, the previous merit function does not work for the polarimeter with $n>4$ modulation states.

According to Eqs. (11) and (12), to make the variances independent of the incident polarization states P, the condition

$$\forall k\in[0,3],\ \|\mathbf{q}_k\|=0 \tag{14}$$

should be first fulfilled. Furthermore, for an optimally balanced instrument matrix, the noise variances on the last three Stokes parameters should be minimized and equal to each other, that is

$$Q_{1,0}=Q_{2,0}=Q_{3,0}. \tag{15}$$

The combination of the conditions in Eqs. (14) and (15) is considered as the optimally balanced condition for Poisson noise (BCPN). The optimal instrument matrix $\mathbf{A}$ for any number $n\geq 4$ of modulation states (except for $n=5$, because there is no optimal modulation states [38–41]) could be determined with the BCPN.

4. Optimization of general polarimeters

To verify the feasibility of the metric BCPN, we first design and optimize general polarimeters that consist of different numbers of modulation states at a single wavelength. As stated previously [38–41], a general polarimeter consisting of a rotatable or variable retarder followed by a fixed polarizer can only reach the optimal values of the EWV, CN or PME. In contrast, a general polarimeter that consists of two variable retarders in tandem followed by a fixed polarizer can achieve the immunity of Poisson noise [45]. The retarders could be liquid crystal variable retarders (LCVRs) with electronically tuned retardances, ferroelectric liquid crystals with electronically switched azimuths, or crystal retarders with mechanically rotated azimuths. As an example, we will optimize the polarimeter that consists of two rotatable quarter waveplates (QWPs) at different numbers of modulation states ($n=4$, 6, 8, 12, 20, 40, 60, 80, 100). These values correspond to the number of the vertexes of the Platonic solids represented on the Poincaré sphere [38, 39]. The variables are the azimuths (θ_1,θ_2) of the two QWPs. The cost function is a linear combination of the conditions in Eqs. (14) and (15) as

$$\varepsilon_1=\sum_{k=0}^{3}\|\mathbf{q}_k\|^2 \tag{16a}$$

$$\varepsilon_2=Q_{1,0}^2+(Q_{2,0}-Q_{1,0})^2+(Q_{3,0}-Q_{1,0})^2, \tag{16b}$$

and

$$(\theta_1,\theta_2)=\arg\min_{\theta}\{\omega_1\varepsilon_1+\omega_2\varepsilon_2\}, \tag{17}$$

Optics EXPRESS

where $\omega_1 = \varepsilon_1 / (\varepsilon_1 + \varepsilon_2)$ and $\omega_2 = \varepsilon_2 / (\varepsilon_1 + \varepsilon_2)$ are adaptive weight factors. While the first term minimizes the influences of the Poisson noise and polarization states, the second term minimizes and balances the influence of the Gaussian noise. A local optimization algorithm, gradient descent method, is applied to determine the optimal polarimeter at different numbers n of modulation states. The optimization process is repeated for many steps at each modulation number n. The initial azimuths for the two QWPs are random in the first step. The generated azimuths are then used as new initial values in subsequent steps. The azimuths that produce the optimal BCPN and its corresponding instrument matrix $\mathbf{A}$ are the solution of the optimization process. The metrics corresponding to the instrument matrix $\mathbf{A}$ at different numbers of modulation states are calculated in Fig. 2.

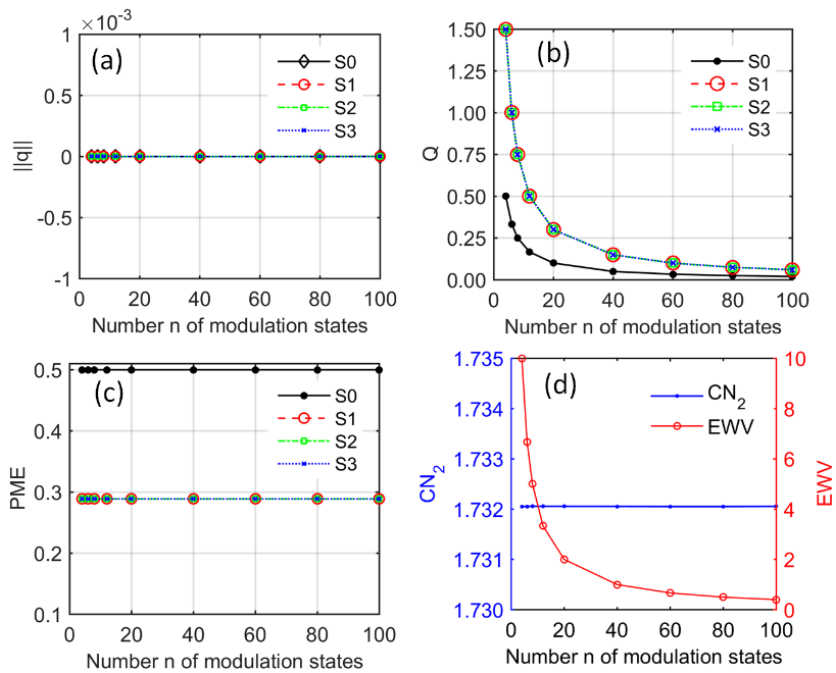

Fig. 2. Different metrics vary with the number n of modulation states when a polarimeter consisting of two QWPs followed by a fixed polarizer is optimized with the metric BCPN.

It is found that $\|\mathbf{q}_k\|$ approaches to zero at different numbers of modulation states as shown in Fig. 2(a), meaning the determined polarimeters have immunity to the Poisson noise. The following relationships are observed from Fig. 2(b) as

$$\forall k \in [1,3],\ \ Q_{k,0} = 3\,Q_{0,0},\ \ \text{and}\ \ \sum_{k=0}^{3} Q_{k,0} = 20/n. \tag{18}$$

The optimal $Q_{k,0}$ decreases with the number n. The figures of merit, EWV, CN and PME, also approach their ideal values as shown in Figs. 2(c) and 2(d) [38–41], meaning the optimal polarimeters have immunity to Gaussian noise. The BCPN can be used for balancing both the Poisson and Gaussian noise. Since the previous analytical solution showed that the optimal $\text{EWV} = 40/n$ [40], so $Q_{k,0}$ are fundamentally related to the EWV, CN and PME. In other word, any figure of merit, EWV, CN or PME, also can get optimal solution for both Gaussian and Poisson noise by linearly combining with the condition in Eq. (14).

Optics EXPRESS

5. Design and optimization of broadband polarimeters

5.1 Error functions and optimization parameters

In this section, we will use the BCPN in Eqs. (14), (15) and (18) to optimize broadband polarimeters. The numerical optimization is evaluated with the error functions over a specific waveband as

$$\Delta\varepsilon_{\mathrm{BCPN}} = \sqrt{\left\langle \sum_{k=0}^{3} \left(\left\| \mathbf{q}_k \right\|^{*} - \left\| \mathbf{q}_k \right\| \right)^2 \right\rangle_{\lambda}} \tag{19a}$$

and

$$\Delta\varepsilon_{Q} = \sqrt{\left\langle \sum_{k=1}^{3} \left(Q_{k,0} - 3Q_{0,0} \right)^2 \right\rangle_{\lambda}} . \tag{19b}$$

where $<\cdot>$ denotes ensemble averaging over the whole wavelength, $\left\| \mathbf{q}_k \right\|^{*} = 0$ is the ideal values for the optimized modulator. The linear combination of these two functions is the final merit function as

$$\Delta\varepsilon = \omega_{\mathrm{BCPN}} \Delta\varepsilon_{\mathrm{BCPN}} + \omega_{Q} \Delta\varepsilon_{Q} , \tag{20}$$

where $\omega_{\mathrm{BCPN}} = \Delta\varepsilon_{\mathrm{BCPN}} / (\Delta\varepsilon_{\mathrm{BCPN}} + \Delta\varepsilon_{Q})$ and $\omega_{Q} = \Delta\varepsilon_{Q} / (\Delta\varepsilon_{\mathrm{BCPN}} + \Delta\varepsilon_{Q})$ are adaptive weight factors. Usually, the retarder stacks consist of a set of retarders (passive or active), and each retarder can be considered as a zero-order QWP at a specific wavelength λ^0 with azimuth θ^0. Then the retardance at other wavelength will be $\delta(\lambda) = \pi\lambda^0 \Delta n(\lambda) / [2\lambda \Delta n(\lambda^0)]$, where Δn is the birefringent index. Based on this operation, the optimization parameters will be

$$\left(\boldsymbol{\lambda}^0 , \boldsymbol{\theta}^0 \right) = \underset{(\boldsymbol{\lambda}, \boldsymbol{\theta})}{\arg\min} \left\{ \Delta\varepsilon \right\} , \tag{21}$$

where ($\boldsymbol{\lambda}$, $\boldsymbol{\theta}$) are vectors that indicate a set of physically admissible wavelengths and azimuths. The optimization algorithm and process are similar to that in Section 4. $\boldsymbol{\lambda}^0$ can be replaced with thickness or retardance of individual retarder, because they fundamentally relate to each other. During optimization, the retarder stack is not arranged as a Pancharatnam type or Pancharatnam-like type [16], both the retardance and azimuth are flexible for optimization as we did previously [26]. For the convenience of assembling and alignment, the azimuth of the first retarder is usually fixed at 0°. The spectral sampling is equidistant in the wavenumber domain to avoid under sampling at short wavelength [31].

5.2 The choice of modulation states

Usually, the method to build the retarder stack and to find optimal values of the parameters (λ, θ) depends on the number n and the distribution of the modulation states. As stated in Section 2, the retarder stack acts as an equivalent retarder and rotator combination at each wavelength. The possible and fastest way to find optimal value should include two steps:

(i) The first step is to determine whether there is a combination of a retarder and a rotator that works for the selected optimization metric with the specific number n of modulation states at a single wavelength.

(ii) If the combination exits, the second step is to select the number of retarders in a retarder stack and use Eq. (21) to realize the function of such combination over the whole

Optics EXPRESS

wavelength and determine the optimal values ($\boldsymbol{\lambda}^0$, $\boldsymbol{\theta}^0$). The number of retarders in the retarder stack increases gradually to find the best solution. While fewer retarders are better for fabrication and assembling, more retarders are better for error reduction.

It is well-known that $n = 4$ modulation states is the least number to demodulate the incident Stokes vector. Division-of-aperture and division-of-focal-plane snapshot imaging polarimeters usually employ four modulation states to achieve maximum spatial resolution on a single array detector [46–50]. For the optimization metrics CN, EWV and PME, there is an optimal retarder and rotator combination as pointed in reference [25, 38–41]. The combination includes a 0° rotator and a 132° retarder, and rotates to four angles (± 51.7°, ± 15.1°) respectively. The retarder stack for this combination was achieved over the visible region [26]. However, these combinations are not valid for the metric BCPN [41, 45].

For the $n > 4$ modulation states, there exists a combination that works for the optimization metrics CN, EWV and PME [40]. The retarder stacks for achieving the function of the combination were proposed in references [29–36]. However, the combination is not valid for the metric BCPN either.

One of the methods to satisfy the metric BCPN for $n = 4$ modulation states is to use two different combinations, and each combination produces two modulation states [45]. As we reported previously [45], the first combination includes a 0° rotator and a 102° retarder, and the combination rotates to ± 72° respectively. The second combination includes a 0° rotator and a 142° retarder, and the combination rotates to ± 35° respectively. This method also works for any above mentioned optimization metric (CN, EWV or PME). As an example, the two retarder stacks to achieve the function of the combinations will be presented in Section 6. The drawback of using these two combination is that it is not convenient to develop a division-of-time polarimeter architecture, because the two combinations should be exchangeable to produce all of four modulation states. In contrast, it is convenient to develop a division-of-amplitude, a division-of-aperture, or a division-of-focal-plane polarimeter architecture, because all of modulation states work in parallel.

Another method to satisfy the metric BCPN for $n = 4$ modulation states is to use two separate combinations. However, the two combinations should work in tandem for each modulation state and rotate to different angles simultaneously. If both the combinations are equivalent to QWPs, they should be rotated to four pairs of rotation angles (± 70.2°, ± 87.8°) and (± 42.8°, ± 19.1°) [45]. This method also works for any above mentioned optimization metric (CN, EWV or PME) and any number $n > 4$ of modulation states.

6. Optimization examples and discussion

For the broadband polarimeter integrated with a number of retarders, usually there are ripples in the transmitted polarization spectra resulting from the interference of the internal multiple reflections between the parallel surfaces of the retarders (Fabry-Pérot etalon effect) [51, 52]. However, retarders made of the same material can avoid severe ripples [17, 18]. As an example, a stack of retarder plates made of crystal quartz that is transparent over a relatively wide waveband is employed in the polarimeter. The birefringence of the quartz is calculated with the Sellmeier formula [53]. Since the true zero-order waveplate is too thin to be polished with current technologies, it can be replaced by the multi-order or compound quasi zero-order waveplate after getting the optimal parameters ($\boldsymbol{\lambda}^0$, $\boldsymbol{\theta}^0$). Although the quartz plate can be cemented on an optical glass substrate and then polished to the true zero-order waveplate, the optical glass will introduce transitions in refractive index and thus increase the polarized spectral fringes in the transmitted spectra. In the following examples, the parameters ($\boldsymbol{\lambda}^0$, $\boldsymbol{\theta}^0$) are optimized over the visible-to-infrared wavelength region of 0.38 - 1.1 μm which is randomly selected. Theoretically, the optimization can be implemented within the spectral window of retarder' material. The design goal is to make the maximum spectrally averaged error no more than 5%, i.e. $\Delta\varepsilon \le 0.05$, with 200 samples.

Optics EXPRESS

In this section, we optimize the retarder stack using Eqs. (19)-(21) for $n=4$ modulation states. According to the approach in Section 5.2, two different retarder stacks should be designed for two pairs of modulation states. The first retarder stack $\#1$ is rotated to the angles ± 72°, and the second $\#2$ is rotated to angles ± 35°. The maximum spectrally averaged errors $\Delta\varepsilon_{\mathrm{BCPN}}$ for different numbers of retarder plates are summarized in Table 1.

Table 1. The maximum spectrally averaged errors from the optimization of broadband polarimeter using the metrics BCPN. The polarimeter includes two different retarder stacks and each stack consists of *m* retarders to produce two modulation states after rotation.

	$m=3$	$m=4$	$m=5$	$m=6$	$m=7$	$m=8$	$m=9$
$\Delta\varepsilon_{\mathrm{BCPN}}$	39.0%	35.2%	10.7%	10.3%	5.57%	5.34%	2.46%
$\Delta\varepsilon_{\mathrm{PME}}$	3.11%	3.48%	2.54%	2.45%	0.84%	0.87%	0.46%
$\Delta\varepsilon_{\mathrm{EWV}}$	55.2%	60.5%	20.4%	18.4%	3.32%	4.02%	0.75%
$\Delta\varepsilon_{\mathrm{CN}_2}$	27.4%	30.2%	14.2%	13.5%	5.05%	5.16%	2.17%

For comparison, the maximum spectrally averaged errors for other three metrics are also evaluated respectively with

$$\Delta\varepsilon_{\mathrm{CN}_2}=\sqrt{\left\langle\left(\mathrm{CN}_2^*-\mathrm{CN}_2\right)^2\right\rangle_\lambda}, \tag{22}$$

$$\Delta\varepsilon_{\mathrm{EWV}}=\sqrt{\left\langle\left(\mathrm{EWV}^*-\mathrm{EWV}\right)^2\right\rangle_\lambda}, \tag{23}$$

and

$$\Delta\varepsilon_{\mathrm{PME}}=\sqrt{\left\langle\left(\mathrm{PME}_0^*-\mathrm{PME}_0\right)^2+\sum_{k=1}^{3}\left(\mathrm{PME}_k^*-\mathrm{PME}_k\right)^2\right\rangle_\lambda}, \tag{24}$$

where $\mathrm{CN}_2^*=\sqrt{3}$, $\mathrm{EWV}^*=40/n$, $\mathrm{PME}_0^*=1/2$, and $\mathrm{PME}_k^*=1/2\sqrt{3}$ are the ideal values for the optimized modulator respectively.

As shown in Table 1, only the retarder stack that includes more than $m=7$ retarders can meet the requirement of the maximum error in the BCPN. Under this situation, the errors in the other three metrics also satisfy the requirement. However, the retarder stack with only $m=3$ plates already can ensure the requirement of the metric PME, meaning the requirement of the metric BCPN is tighter than the metric PME. No obvious performance improvement for the retarder stack of the even number m to that of the odd number $(m-1)$.

For the retarder stack with $m=9$ retarders, the optimal values ($\boldsymbol{\lambda}^0$, $\boldsymbol{\theta}^0$) of the two retarder stacks are listed in Table 2. The corresponding spectral distributions of the four metrics are plotted in Fig. 3. It is found that the resulted instrument matrix $\mathbf{A}$ at each wavelength is similar to the ideal matrix in Eq. (13). That means broadband polarimeter has the similar polarimetric properties over the whole wavelength region. Therefore, it can be considered as an achromatic one. This is different from the polychromatic retarders optimized from the metric PME [27–36].

The difference can be explained physically. For any number *n* of modulation states, there is only a unique instrument matrix (such as the ideal instrument matrix in Eq. (13) for $n=4$) which can fulfill the requirement of the metric BCPN and has immunity to Poisson noise. The optimal solution $\mathbf{A}$ at each wavelength should be similar to Eq. (13), and the only way is to produce achromatic retarders.

Optics EXPRESS

In contrast, it is not necessary to have a fixed instrument matrix to fulfil the requirement of the metric PME. It is well-known that the number n of modulation states corresponds to the vertexes of a polyhedrons that represented upon the Poincaré sphere [21, 25, 38, 39, 44]. Only regular polyhedrons can maximize the Poincaré sphere enclosed volume and result in polarimeters whose noise propagation of the intensity measurements is minimized. However, the orientation of the regular polyhedrons are variable, and different orientations means different instrument matrixes [38, 39].

Table 2. The optimal values (λ^0, θ^0) of the two retarder stacks with m = 9 retarders.

		p = 1	p = 2	p = 3	p = 4	p = 5	p = 6	p = 7	p = 8	p = 9
#1	λ^0 (μm)	0.855	0.947	0.889	1.081	1.076	0.654	0.786	0.743	0.832
	θ^0 (deg)	0	27.5	38.6	–47.6	–43.5	10.5	–21.1	62.6	72.8
#2	λ^0 (μm)	0.813	1.018	1.020	1.009	0.993	1.035	1.033	1.000	1.010
	θ^0 (deg)	0	53.9	–4.1	15.6	–63.3	–51.7	19.9	5.3	70.4

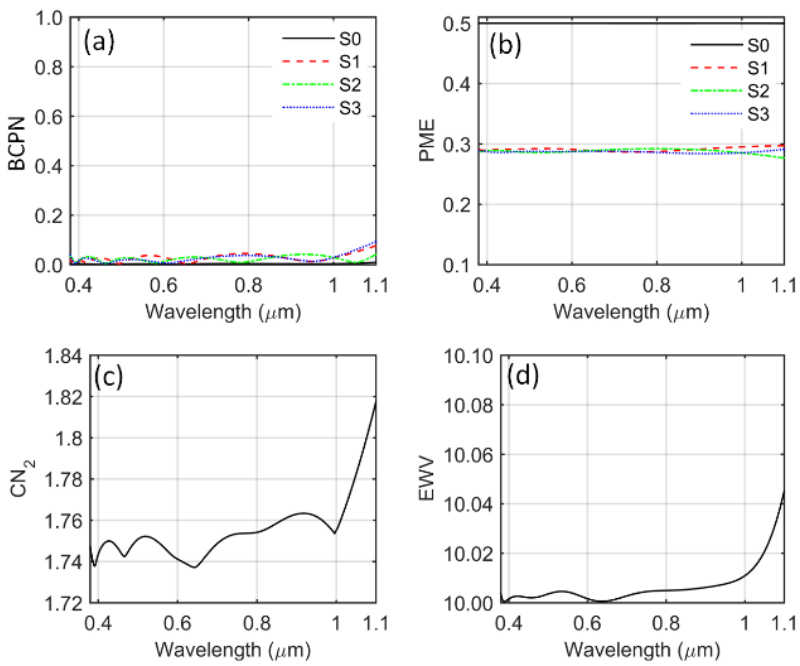

Fig. 3. The results optimized from the metric BCPN. The corresponding metrics (a) BCPN, (b) PME, (c) CN_2 and (d) EWV for the broadband polarimeter with four modulation states. Each two states are produced by a retarder stack that includes nine retarders as presented in Table 2.

The achromatic behavior can be revealed by the equivalent retardance Φ and azimuth α of the resulted retarder and the equivalent rotation angle β of the resulted rotator that is represented in Eq. (3) and depicted in Fig. 4. Obviously, the first retarder stack #1 is equivalent to a 102° retarder. Although the resulting retardance Φ has large vibration, the azimuths (α, β) of the resulting retarder and rotator are close to zero. The second retarder stack #2 is equivalent to a 142° retarder. In contrast, the resulting retardance approaches to the ideal value, the azimuths of the resulted retarder and rotator have considerable vibrations. It demonstrates two quasi-achromatic retarders are the best solutions for the metric BCPN.

Since the retarder stacks act as achromatic retarders, we can also design two achromatic retarders directly with the function,

Optics EXPRESS

$$\left(\lambda^0, \theta^0\right) = \underset{(\lambda,\theta)}{\arg\min}\left\{\sqrt{\left\langle\left(\Phi^* - \Phi\right)^2 + \left(\alpha^* - \alpha\right)^2 + \left(\beta^* - \beta\right)^2\right\rangle_\lambda}\right\}, \tag{25}$$

and then rotate them to angles ± 72° and ± 35° respectively. However, this method is not as efficient as the previous one, because it cannot account for the cooperation of the azimuths and retarders in the two retarder stacks [26].

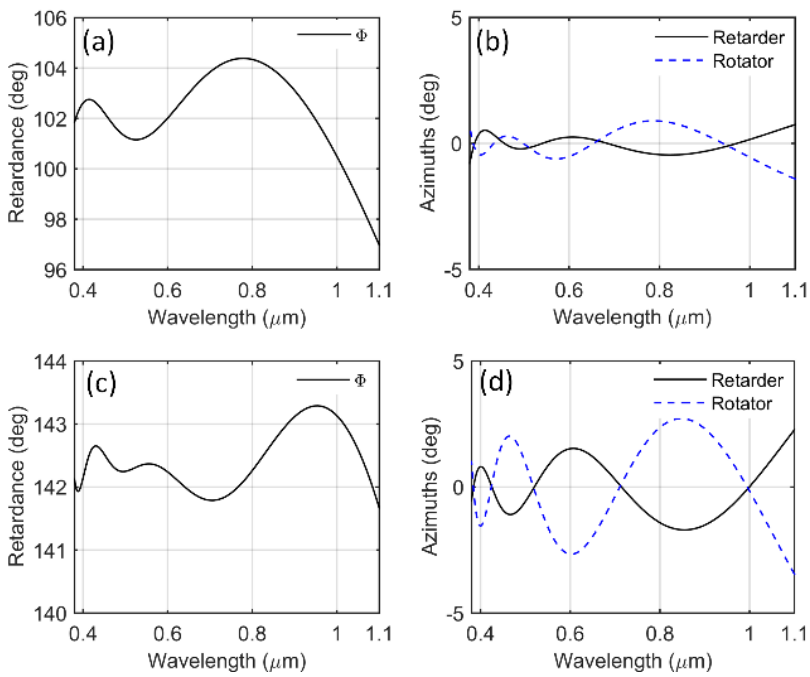

Fig. 4. The results optimized from the metric BCPN. (a) The equivalent retardance of the resulted retarder and (b) the equivalent azimuth and rotation angle of the resulted retarder and rotator for the first retarder stack #1. (c) The equivalent retardance of the resulted retarder and (d) the equivalent azimuths of the resulted retarder and rotator for the second retarder stack #2.

7. Conclusion

In summary, we have proposed a new paradigm for the design and optimization of a broadband polarimeter with immunity to both Gaussian and Poisson noise. While the CN, EWV, PME only optimally balance the Gaussian noise in the polarimeter, the proposed BCPN accounts for both Gaussian and Poisson noise. For the optimizations with the metrics CN, EWV and PME, there will be a number of feasible solutions and only a few of them can satisfy the BCPN. However, it is hard to determine these special solutions for the BCPN. In contrast, by using the BCPN directly to optimize the retarder stacks, the optimal results are also applicable to the CN, EWV and PME. However, more retarders in each retarder stack are needed to fulfill the error tolerance of the BCPN. While the polarimeter optimized from the CN, EWV and PME is recognized as a polychromatic one, the polarimeter optimized from the BCPN can be achromatic.

At least two retarder stacks are required to satisfy the requirement of BCPN over a wide waveband. If the passive elements made of Mica, quartz, MgF_2, or sapphire are used to design the polarimeter, the two retarders or two retarder stacks should be separated completely. It would be hard to reduce the number of retarders in each retarder stack. However, if the active elements such as photoelastic polarimeters, Pockels cells, nematic or ferroelectric liquid crystals are used to design the broadband polarimeter, the two retarder stacks may cooperate

Optics EXPRESS

with each other and it may be possible to reduce the number of retarders in each retarder stack. In future work, we will develop the broadband polarimeter with the active elements and use the minimum amount of elements in each retarder stack for a specific number of modulation states.

Funding

China Scholarship (201406285048); Fundamental Research Funds for the Central Universities of China (xjj2013044); Specialized Research Fund for the Doctoral Program of Higher Education of China (20130201120047); Natural Science Basic Research Plan in Shaanxi Province of China (2014JQ8362); National Natural Science Foundation of China (NSFC) (41530422, 61275184, 61405153, 61540018); National Major Project (32-Y30B08-9001-13/15).

150.135.119.195 {ts '2017-03-30 16:32:21'}